

PtSSe/AlN heterojunctions with favorable photogenerated currents and structural stability

Zhen Cui(崔真), Lannan Yan(鄢岚楠), Yuqiao Ren(任语乔), Junliang Yao(姚俊良), and Chenxing Liu(刘晨兴)
Citation: Chin. Phys. B, 2026, 35 (**6**): 067305. DOI: 10.1088/1674-1056/ae3db7
http://cpb.iphy.ac.cn; http://iopscience.iop.org/cpb

What follows is a list of articles you may be interested in

First principles prediction of the valley Hall effect in ScBrCl monolayer

Xiang Yu(于翔), Ping Li(李萍), and Chang-Wen Zhang(张昌文)
Chin. Phys. B, 2025, 34 (**4**): 047305. DOI: 10.1088/1674-1056/adbacb

Diamond/c-BN van der Waals heterostructure with modulated electronic structures

Su-Na Jia(贾素娜), Gao-Xian Li(李高贤), Nan Gao(高楠), Shao-Heng Cheng(成绍恒), and Hong-Dong Li(李红东)
Chin. Phys. B, 2023, 32 (**7**): 077301. DOI: 10.1088/1674-1056/acac10

First principles study on geometric and electronic properties of two-dimensional Nb_2CT_x MXenes

Guoliang Xu(徐国亮), Jing Wang(王晶), Xilin Zhang(张喜林), and Zongxian Yang(杨宗献)
Chin. Phys. B, 2022, 31 (**3**): 037304. DOI: 10.1088/1674-1056/ac322e

High-throughput identification of one-dimensional atomic wires and first principles calculations of their electronic states

Feng Lu(卢峰), Jintao Cui(崔锦韬), Pan Liu(刘盼), Meichen Lin(林玫辰), Yahui Cheng(程雅慧), Hui Liu(刘晖), Weichao Wang(王卫超), Kyeongjae Cho, and Wei-Hua Wang(王维华)
Chin. Phys. B, 2021, 30 (**5**): 057304. DOI: 10.1088/1674-1056/abdb1a

Enhanced thermoelectric properties in two-dimensional monolayer Si_2BN by adsorbing halogen atoms

Cheng-Wei Wu(吴成伟), Changqing Xiang(向长青), Hengyu Yang(杨恒玉), Wu-Xing Zhou(周五星), Guofeng Xie(谢国锋), Baoli Ou(欧宝立), and Dan Wu(伍丹)
Chin. Phys. B, 2021, 30 (**3**): 037304. DOI: 10.1088/1674-1056/abd163

PtSSe/AlN heterojunctions with favorable photogenerated currents and structural stability

Zhen Cui(崔真)[1,2,†], Lannan Yan(鄢岚楠)[1], Yuqiao Ren(任语乔)[3], Junliang Yao(姚俊良)[1], and Chenxing Liu(刘晨兴)[1]

[1] *School of Automation and Information Engineering, Xi'an University of Technology, Xi'an* 710048, *China*
[2] *Xi'an Key Laboratory of Wireless Optical Communication and Network Research, Xi'an University of Technology, Xi'an* 710048, *China*
[3] *School of Electronic Science and Engineering, Xi'an Jiaotong University, Xi'an* 710049, *China*

(Received 14 October 2025; revised manuscript received 20 January 2026; accepted manuscript online 27 January 2026)

A comprehensive first-principles and density functional theory study was conducted to explore the band structure, differential charge redistribution, optical properties, and photoelectric detection characteristics of PtSSe/AlN heterojunctions. The results identify the PtSSe/AlN heterojunction as a structurally stable, type-II semiconductor, demonstrating an indirect bandgap of 1.53 eV, and representing a typical van der Waals heterojunction capable of efficient electron–hole pair separation. The internal electric field induced by the interface serves to lower the barrier height, thus promoting carrier injection. The application of strain maintains the type-II band alignment, ensuring high stability. Meanwhile, PtSSe/AlN heterojunctions have good light-harvesting capability in the ultraviolet to visible spectrum, exhibiting three pronounced absorption peaks within the visible spectral range. The self-powered photodetector based on this heterojunction achieves high photocurrent density under different polarized lights; when the incident light energy is 2.6 eV, the maximum value of the extinction coefficient is about 14. The results indicate the device's versatility for applications, including in photoelectric detectors, optical modulators, and sensors. This research provides theoretical foundations for developing novel photodetectors, establishes a robust basis for experimental studies and device fabrication, and holds promise for advancing high-performance multifunctional optoelectronic devices.

Keywords: PtSSe/AlN, first principles, heterojunction photodetector, extinction ratio

PACS: 73.40.Lq, 78.20.Jq, 82.47.Jk

DOI: 10.1088/1674-1056/ae3db7 **CSTR:** 32038.14.CPB.ae3db7

1. Introduction

Two-dimensional (2D) materials have gained significant traction across numerous technical disciplines, driven by their exceptional properties. Representative 2D materials, including graphene,[1] gallium nitride (AlN),[2] black phosphorus (P),[3] and transition metal dichalcogenides (TMDs),[4] have been widely applied in optoelectronics, environmental, energy, aerospace, and other fields as a result of their peculiar atomic configuration and resulting functional characteristics.[5]

It has been found that stacking van der Waals materials can be used to explore a range of rich physical phenomena. Yang *et al.*[6] studied the structure, electronic behavior, and light-absorption characteristics of blue-phosphorene/graphene-like AlN composites. They discovered that in the heterojunction the conduction band minimum (CBM) and valence band maximum (VBM) reside in different monolayers, leading to enhanced photocatalytic efficiency. Hao *et al.*[7] fabricated a lateral Ga_2O_3/AlN heterojunction. Under zero bias voltage, it was found that a dark current of 1.45×10^{-13} A and a UV switching ratio of 2.14×10^4; the light response was 95.95 mA/W. The photodetector demonstrated a temporal response of 90 ms for rise and 116 ms for decay, indicating a rapid response capability. The internal electric field of the device enables self-powered operation and facilitates effective charge separation. Liu *et al.*[8] constructed a van der Waals heterostructure photodetector using 2D molybdenum disulfide and AlN. They found that the polarization effect of AlN could enhance the optical properties of molybdenum disulfide. In addition, a 3 nm thick alumina layer was deposited on molybdenum disulfide to study the strain effect. The results showed that under 365 nm illumination the strained device exhibited significantly improved performance compared with the control device, with photocurrent and responsivity increasing more than fivefold. Xu *et al.*[9] investigated AlN/β-Ga_2O_3 heterojunction photodetectors and revealed that the heterojunction achieved a response time as fast as 320 ms while operating at 0 V. The device delivered 7.0 mA of signal current per watt of incident light and could spot signals as faint as 1.25×10^{13} Jones. Kumar *et al.*[10] fabricated photodetectors with n-MoS_2/p-Si and n-MoS_2/AlN/P-Si heterojunctions using DC magnetron sputtering technology.[11] The heterojunctions exhibited responsivities of 0.3378 A/W and 1.865 A/W under 532 nm visible light illumination, and reached 0.1245 A/W and 1.4743 A/W under 1064 nm near-infrared radiation, respectively. Notably, inserting an ultrathin AlN insulating layer sped the device up, cutting the rise

†Corresponding author. E-mail: zcui@xaut.edu.cn

© 2026 Chinese Physical Society and IOP Publishing Ltd. All rights, including for text and data mining, AI training, and similar technologies, are reserved.

and fall times from 47.30 μs and 56.58 μs to just 3.32 μs and 4.73 μs, respectively.

Gao and colleagues[12,13] investigated a sunblind avalanche photodetector based on a β-Ga_2O_3/AlN n-Si heterostructure. They found that the AlN layer served as a lattice adaptor between β-Ga_2O_3 and Si, reducing the dark current of the device. When the optical power density was 4.81 μW/cm^2, the device achieved performance metrics as high as 131.3 A/W for responsivity and 2.9×10^{15} Jones for detectivity. The high gain enabled the device to maintain excellent performance even under weak UV light (0.119 W/cm^2), achieving 342.7 A/W and 3.2×10^{14} Jones, respectively, at −85 V. Fan *et al.*[14] examined the robustness of AlN/B_2SSe stacks, their band alignment, optical absorption and emission, and photocatalytic driving performance. Their study revealed that the work function of B_2SSe (6.31 eV) exceeded that of AlN (5.81 eV), indicating electron transfer from the AlN to the B_2SSe layers during heterojunction formation until Fermi-level equilibrium was achieved, thereby creating an intrinsic interlayer electric field. Furthermore, the light absorption range in model III of the AlN/B_2SSe heterostructure was extended to 557 nm, while in model IV it expanded to 683 nm.

In addition, TMDs lack inversion symmetry, which endows them with an intrinsic dipole that sets up a perpendicular built-in field, efficiently splitting photogenerated electron–hole pairs. TMDs have also attracted extensive research interest as an alternative class of photocatalytic materials. $PtSe_2$ possesses a dual semiconducting–metallic character, distinguishing it from other TMDs. A semiconductor-to-semimetal transition in $PtSe_2$ is realized once the stacking advances from a double layer to a multilayer regime. Zhao *et al.*[15] studied the $PtSe_2$/$ZrSe_2$ heterojunction. Their findings reveal that the band alignment of the heterojunction can be toggled between type-I and type-II simply by varying the stacking geometry, while its electronic character remains highly susceptible to both interlayer coupling and external electric fields. In addition, under the influence of an external electric field, the band gap can be tuned in the range of 0–0.25 eV. Shahid *et al.*[16] investigated the Bi_2Se_3/$PtSe_2$ heterojunction, demonstrating that the van der Waals heterostructure integrating multiple layers of Bi_2Se_2 and $PtSe_2$ exhibits tunable carrier and spin dynamics via compositional modulation. Zhao *et al.*[17] investigated the van der Waals heterojunction of $PtSe_2$/$SnSe_2$, revealing a significantly reduced band gap compared with its constituent materials. Their study demonstrated that this band gap exhibits exceptional sensitivity to interlayer coupling and X-axis strain. Notably, the heterojunction transitions from a semiconductor to a metallic state under applied stress, suggesting promising applications in optoelectronic detectors and solar cells.

PtSSe is a TMD that can be synthesized through sulfidation treatment of single-layer $PtSe_2$ under a hydrogen sulfide gas flow. Monolayer PtSSe has been theoretically shown to possess a favorable band gap, strong visible-light harvesting, and well-aligned band edges. Jakhar *et al.*[18] found that the photoelectric properties of transition metal sulfides can be regulated by strain, electric field, and surface doping. Compared with conventional 2D MX_2 compounds, PtSSe monolayers are intrinsically asymmetric and their built-in dipole moments efficiently drive charge-carrier separation throughout the photocatalytic cycle. Xie and colleagues[19,20] designed a van der Waals heterojunction of SnS_2 and PtSSe based on the single-layer design of SnS_2 and PtSSe. Experimental results demonstrate that the heterojunction exhibits excellent structural stability. Featuring a typical type-II band structure, it facilitates the separation of photoexcited charge carriers into distinct regions. Piling up of interfacial charge sets up a built-in field oriented from SnS_2 to PtSSe, driving electrons and holes into opposite layers and thereby enhancing photocatalytic efficiency. Pang *et al.*[21] investigated the stacked structure and electronic, optical, and catalytic properties of a vertical heterojunction constructed from graphene-like C_6N_6 layers and PtSSe single layers.[22] The results show that the selenium side contact g-C_6N_6/PtSSe heterojunction is a typical type-II semiconductor material. Jamdagni *et al.*[23] investigated the PtSSe van der Waals heterojunction, which showed a stable type-II band arrangement with an optimal stacking configuration. The interlayer band gaps between adjacent layers near the band edges facilitate carrier recombination between the CBM and VBM layers. This enhanced spatial charge separation capability significantly improves the performance of Z-type heterostructures.

Based on the first-principles method,[24,25] the aim of this work is to construct a PtSSe/AlN heterostructure and explore its band structure properties. First, the positions of PtSSe and Al atoms are finely adjusted on AlN, and six different configurations of PtSSe/AlN heterojunctions are successfully obtained. The core objective of this operation is to achieve effective separation of electrons and holes, laying the foundation for subsequent high-performance photoelectronic applications. Then, optimization of these six configurations is carried out and the most stable stacking structure is selected from them.[26] The determination of this stable structure is an important basis for subsequent research, because the stability of the structure directly affects performance. Next, the most stable PtSSe/AlN heterostructure is systematically examined to gather a comprehensive range of its properties. In the study of electronic properties, we focus on key parameters such as electron transfer, band structure, and work function. In terms of optical properties, the formation of the heterojunction results in a widened optical absorption range and a marked boost in intensity relative to the constituent materials. For charge

transfer, a method using plane electrostatic potential, Bader charge, and combined three-dimensional charge density distribution is used for a comprehensive analysis to accurately determine the charge transfer. Finally, for the PtSSe/AlN heterojunction self-powered photodetector, the photocurrent and extinction ratio under linearly polarized light (LPL) and elliptically polarized light (EPL) are calculated. The results show that the PtSSe/AlN heterostructure is polarization insensitive and has a high extinction ratio, making it highly relevant for photodetection applications.

2. Computational methods

The computational model of the heterojunction is constructed from a single layer of PtSSe and AlN stacked vertically in the crystal cell. At the same time, a vertical 20 Å vacuum layer is added to ensure the 2D nature of the structure. The geometry of the PtSSe/AlN heterojunction system was optimized by density functional theory (DFT).[27] The Vienna *Ab initio* Simulation Package was used to perform relevant calculations using DFT. The calculations employed a plane-wave basis set with projector augmented wave potentials in conjunction with the Perdew–Burke–Ernzerhof generalized gradient approximation. The HSE06 method[28] was employed for its exceptional accuracy in predicting electronic properties. Calculations used a 500 eV wave cutoff and a $4000 \times 4000 \times 1000$ grid for both the PtSSe/AlN heterostructure and the free-standing PtSSe and AlN cells. The convergence threshold for the structural and electronic relaxations was set to 10^{-7} eV for the energy and 10^{-3} eV/Å for the atomic forces. Weak dispersion interactions were included using the Grimme DFT-D3 method,[29] and the Brillouin zone was sampled using the Monkhorst–Pack scheme. We also checked how well the stack holds together by running molecular dynamics tests for stability and thermal resistance.[30]

To identify the most stable structure of the PtSSe/AlN heterojunction, we carried out interfacial binding energy calculations on various heterojunction structures. Generally, the system with the smallest interfacial binding energy is the most stable, signifying the ground-state structure. Therefore, by comparing the interfacial binding energies of different configurations, the most stable structure can be identified. The calculation formula is given by [31]

$$E_{\mathrm{b}} = (E_{\mathrm{h}} - E_1 - E_2), \tag{1}$$

where E_{b} is the binding energy of the PtSSe/AlN heterojunction, E_{h} is the total energy of the PtSSe/AlN heterojunction, E_1 is the total energy of a single layer of AlN, and E_2 is the total energy of a single layer of PtSSe.

The interfacial charge redistribution was characterized by calculating the charge density difference and quantified through Bader charge analysis[32]

$$\Delta\rho = \rho_{\mathrm{h}} - \rho_1 - \rho_2, \tag{2}$$

where ρ_{h} is the charge density of the PtSSe/AlN heterojunction, ρ_1 is the charge density of AlN, and ρ_2 is the charge density of PtSSe.

The work function is calculated as follows:[33]

$$\phi = E_{\mathrm{vac}} - E_{\mathrm{F}}, \tag{3}$$

where ϕ is the work function of the material, E_{vac} is the vacuum energy level of the material, and E_{F} is the Fermi energy level of the material.

It is crucial to determine whether solar energy can be used effectively, so the optical absorption of the PtSSe/AlN heterostructure was calculated using the formula for the absorption coefficient (α)[34]

$$\varepsilon(\omega) = \varepsilon_1(\omega) + \mathrm{i}\varepsilon_2(\omega), \tag{4}$$

$$\alpha(\omega) = \frac{\sqrt{2}\omega}{c}\left[\sqrt{\varepsilon_1^2(\omega)+\varepsilon_2^2(\omega)} - \varepsilon_1(\omega)\right]^{\frac{1}{2}}. \tag{5}$$

Here, ω, ε_1, ε_2, and c are the photon frequency, the real part of the complex dielectric constant, the imaginary part of the complex dielectric constant, and the speed of light in a vacuum, respectively.

Finally, the photoelectric current of each heterojunction is computed; the corresponding expression is given by[35]

$$J_{\mathrm{ph}} = \frac{\mathrm{i}e}{\hbar}\int T_{\mathrm{r}}\{\Gamma_{\mathrm{L}}[G^{<(\mathrm{ph})} + f_{\mathrm{L}}(E)(G^{>(\mathrm{ph})} - G^{<(\mathrm{ph})})]\}\,\mathrm{d}E, \tag{6}$$

where $\hbar$ is the Planck constant, Γ_{L} is the coupling coefficient of a port, f_{L} is the Feynman–Dyson function, and $G^{<(\mathrm{ph})}$ is a "lesser (greater) Green function" containing photon–electron interactions.

3. Characteristics of intrinsic materials AlN and PtSSe and model construction

3.1. Research on the properties of AlN and PtSSe intrinsic materials

A detailed investigation of the stacked AlN/PtSSe structures is important for evaluating the geometric structure and electronic properties of the individual constituent materials. Details are shown in Fig. 1. The primary task was to examine the structures of AlN and PtSSe. By employing a $2 \times 2 \times 1$ AlN supercell and a $\sqrt{3} \times \sqrt{3} \times 1$ PtSSe supercell, we constructed a heterostructure with an exceptionally small lattice mismatch of 0.6%, thereby establishing a reliable basis for subsequent studies. High-level calculations yielded accurate lattice constants — monolayer AlN relaxes to 3.12 Å, reproducing Zhao's result within fractions of an angstrom and confirming the present benchmark. Furthermore, the lattice constant of monolayer PtSSe was determined to be 3.58 Å, a

value which is consistent with the findings of Nguyen *et al.*,[36] thereby affirming the reliability of the data.

When considering the formation of a heterostructure between AlN and PtSSe, the lattice mismatch rate becomes a key index for measuring the influence on structural stability and electronic properties. With precise calculation, the lattice mismatch between these two materials was determined to be only 0.6%. A lattice mismatch of less than 5% suggests that the heterostructure remains within a controllable structural range, and its electronic properties are not expected to be significantly affected. This shows that AlN and PtSSe have properties suitable for constructing stable heterostructures, providing a solid theoretical basis for the subsequent construction of PtSSe/AlN heterostacking structures and establishing a platform for further study of various characteristics of this heterostructure.

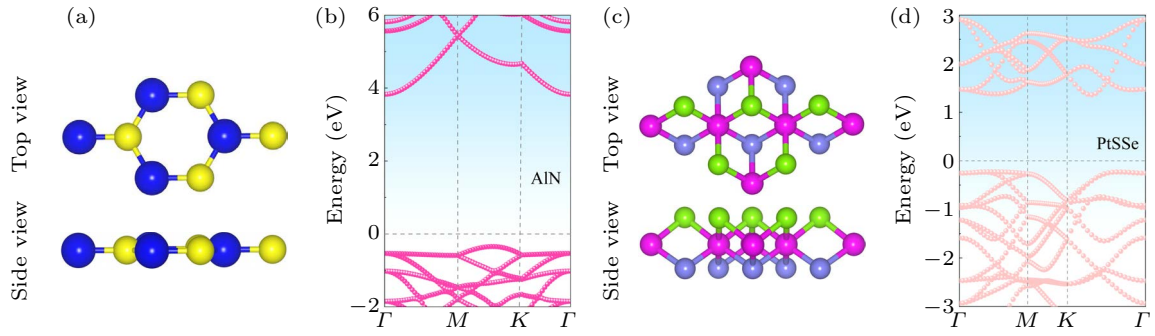


Fig. 1. (a) Crystal structure of single-layer AlN. (b) Band structure of single-layer AlN. (c) Crystal structure of single-layer PtSSe. (d) Calculated band structure of the PtSSe monolayer.

In this study, in order to explore the energy bands of AlN and PtSSe heterostacking structures, the HSE06 method was used. The results are detailed in Fig. 1, which provides results for the structural and band characteristics of both materials. Figure 1(a) shows the geometric structure of a single layer of AlN, namely a typical single-layer plane structure. Figure 1(b) illustrates the band structure of AlN, where the bottom of the conduction band is clearly positioned at point Γ and the top of the valence band is located near the left side of point K. Electronic structure characterization reveals that AlN has an indirect gap with a value of 4.17 eV. When compared with the computational results of Bacaksiz *et al.*,[37] these values show remarkable similarity, further confirming the reliability of this material's bandgap data. Figure 1(c) shows the unique geometric structure of single-layer PtSSe, which is an interlayer structure. As illustrated in Fig. 1(d), monolayer PtSSe exhibits a CBM just to the right of K and a VBM at M. This indicates that PtSSe is also an indirect bandgap semiconductor, with a bandgap value of 1.58 eV. This result aligns closely with the findings of Vo *et al.*,[38] providing a robust reference for subsequent research on PtSSe materials.

3.2. Model construction for the PtSSe/AlN heterostructure

Studies show that asymmetric stacking configurations promote charge transfer and electron–hole pair separation. Based on the characterized properties of monolayer AlN and PtSSe, we constructed six different stacking models using these two materials. In Fig. 2, Al, N, S, Se, and Pt atoms are colored blue, yellow, purple, green, and red, respectively. Six distinct stacking configurations of the AlN/PtSSe heterostructure were constructed and denoted as models 1 to 6. In model 1, the Al and Pt atoms are vertically aligned (Fig. 2(a)). In model 2, the Al atom is positioned directly beneath the S atom (Fig. 2(b)). The configuration of model 3 has an Al atom situated beneath the Pt–S bond. In model 4, the Al atom is situated below the Se atom, and in model 5 it is located beneath the Pt–Se bond. In model 6, the AlN unit is positioned below the hollow site formed by four atoms. These configurations are shown in Figs. 2(d)–2(f), respectively.

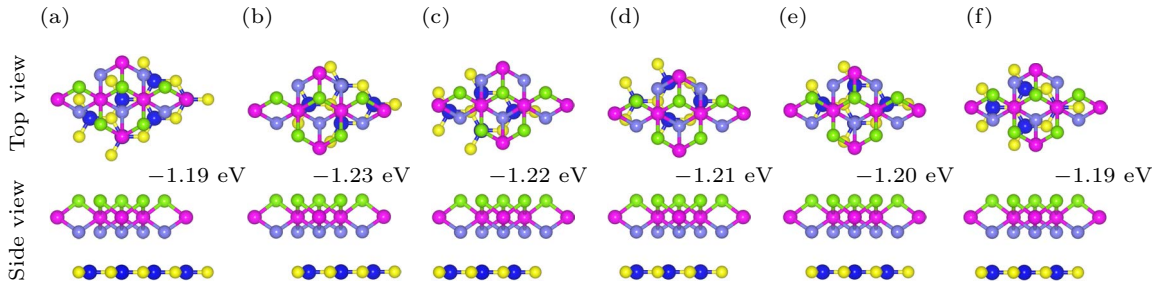


Fig. 2. Six different stacking configurations of the PtSSe/AlN heterojunction.

A comparative study of the binding energies for the six heterostructures was conducted to quantify the relative stability and interfacial interactions in the PtSSe/AlN system. Model 2 emerged as the strongest-bound stack, its −1.23 eV binding energy sitting at the bottom of the energy ladder among the six PtSSe/AlN models. This suggests that the PtSSe/AlN heterostructure is a typical van der Waals heterostructure[39] with an optimized lattice constant of 6.229 Å. All subsequent investigations were conducted based on model 2.

3.3. Results and analysis

3.3.1. Geometry and band structure of the PtSSe/AlN heterostructure

In order to further explore the stability of the PtSSe/AlN heterojunction, molecular dynamics simulation was used to investigate the PtSSe/AlN heterojunction at 300 K. The changes in energy and temperature of the heterojunction over a 3000 fs time range were investigated. During the research, relevant data were generated using professional simulation software. Figure 3 depicts the evolution of the total energy for the PtSSe/AlN heterostructure at 300 K as a function of simulation time from 0 fs to 3000 fs. The constructed supercells are based on the most stable stacking configuration and *ab initio* molecular dynamics simulations for 3000 fs at 300 K. During the simulations, both the total energy and temperature of the system maintained stable fluctuations around their mean values. Figure 3(d) indicates that the system had reached thermal equilibrium. At the microscopic level, there is no breakage of chemical bonds, and at the macroscopic level, there is no structural rearrangement; the overall structure remains intact without obvious damage.

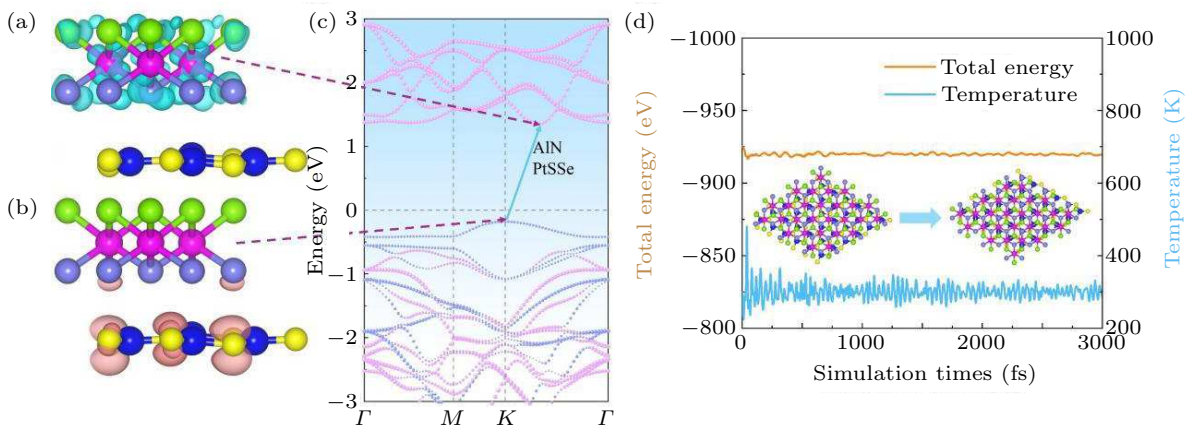


Fig. 3. PtSSe/AlN heterojunction: (a) the CBM, (b) the VBM. (c) Band structure. (d) Computation of molecular dynamics crystal structures and energy changes from scratch at 300 K.

In order to obtain the band structure of the heterojunction accurately, the HSE06 functional is used to study its band structure. Figure 3(c) illustrates a distinctive electronic characteristic of the PtSSe/AlN heterostructure, with its CBM positioned near the *K* point and its VBM residing at the *K* point, and its electronic distribution was further probed through charge density analysis. As observed from Figs. 3(a) and 3(b), the CBM of the PtSSe/AlN heterostructure originates from PtSSe and its VBM is contributed by AlN. This finding indicates that the heterostructure belongs to the type-II band alignment category. This pronounced carrier separation boosts photocatalytic performance and simultaneously positions the PtSSe/AlN heterostructure as a versatile platform for next-generation light-emitting diodes, field-effect transistors, lasers, and logic circuits.

3.3.2. Work function, planar electrostatic potential and planar charge density difference of the PtSSe/AlN heterostructure

The work function is a key parameter that determines the charge redistribution when two semiconductor monolayer materials are made into heterojunctions. Through accurate calculation, the work functions of AlN, PtSSe and PtSSe/AlN are 5.11 eV, 5.33 eV and 4.75 eV, respectively. A comparative analysis of the work functions reveals a lower work function for AlN relative to PtSSe. This difference drives several key physical processes in the PtSSe/AlN heterostructure.

Due to its higher electron affinity, PtSSe attracts electrons from the AlN layer. This electron migration is a process that continues until the Fermi levels equilibrate across the heterojunction. The electron transfer leaves the PtSSe layer electron-rich and the AlN layer electron-deficient, establishing a clear charge polarization and resulting in a clear charge separation across the interface. This built-in electric field plays a critical role in separating electron–hole pairs, leading to improved electrical performance of the material.[40]

In probing the charge transfer mechanism in a PtSSe/AlN heterojunction, the planar electrostatic potential and interfacial potential difference of this material were calculated in detail. The results are shown in Fig. 4(a). The interfacial potential difference of the heterojunction was analyzed in depth, and it

was found that the value reached 7.33 eV, which belongs to the category of a large potential difference. This significant potential difference will affect the band structure of the PtSSe/AlN heterojunction and cause band bending. It effectively lowers the interfacial barrier height within the heterojunction, and the reduction in the barrier height brings many positive effects. The most crucial aspect is that the requisite energy for carrier injection is correspondingly reduced, thereby facilitating the easier injection of carriers into the respective regions. Meanwhile, the carrier diffusion velocity is accelerated, enabling faster movement within the material. This enhanced diffusion rate further improves collection efficiency, allowing more charge carriers to be effectively captured and utilized. Taken together, these modifications give the overall device performance a substantial boost. In the photoelectric conversion process, improved carrier collection efficiency allows more light signals to be converted into electrical signals, thereby boosting conversion efficiency. This breakthrough gives PtSSe/AlN heterojunctions greater potential for applications in optoelectronic devices.[41]

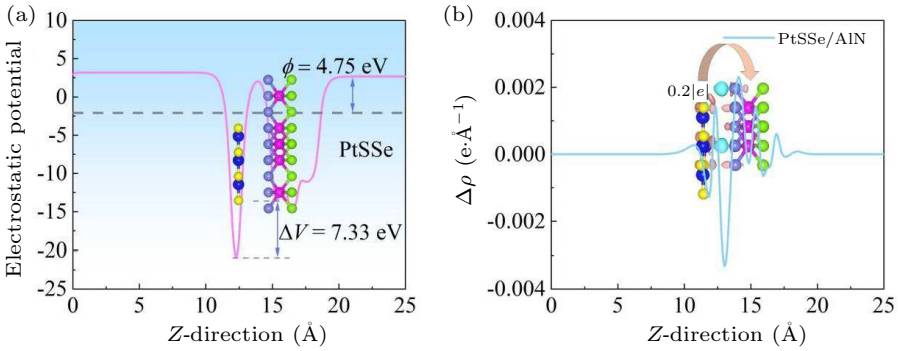


Fig. 4. PtSSe/AlN heterojunction: (a) planar electrostatic potential, (b) planar differential charge density (pink for electron accumulation and cyan for electron depletion).

Figure 4(b) presents the plane-averaged charge-density difference of the PtSSe/AlN heterojunction, providing a quantitative view of the interfacial charge redistribution. The plot reveals that charge accumulates chiefly on the PtSSe side upon junction formation, and Bader analysis quantifies this transfer at $0.2|e|$ from AlN to PtSSe. The electron transfer sharpens transport across the heterojunction, cutting the response time and bolstering stability. The charge and potential data position PtSSe/AlN as a highly promising platform for optoelectronics, photonics, and energy-conversion technologies.

3.3.3. Optical properties of the PtSSe/AlN heterostructure

In investigations of optical performance, the absorption spectrum serves as a key metric for gauging how efficiently a material harvests light.[42] A key observation from Fig. 5 is the limited spectral range of pristine AlN, which absorbs light mostly within the ultraviolet (UV) region compared with the PtSSe/AlN heterostructure. Pristine PtSSe exhibits a relatively broad optical absorption spectrum. However, significant alterations in the optical absorption properties were observed after the construction of the PtSSe/AlN heterostructure; the optical absorption spectra of AlN and PtSSe are significantly broadened, extending from their original absorption regions to the UV, visible, and infrared regions. Notably, three sharp, well-defined peaks appear in the visible range, with the strongest reaching 2.26×10^5 cm^{-1}. This clear boost shows that stacking the two monolayers cures their individual light-harvesting shortcomings, giving the heterostructure much broader and stronger absorption across the spectrum.

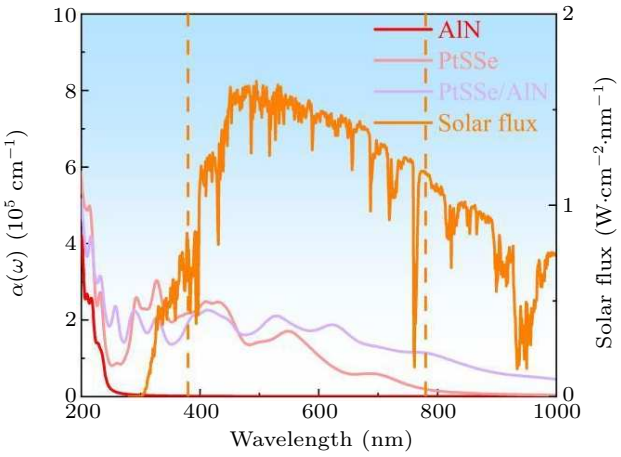


Fig. 5. Optical absorption spectra of AlN, PtSSe, and PtSSe/AlN.

The broadening of the light absorption range and the increase of the absorption peak are of great significance for performance improvement of photoelectric devices. On one hand, it enhances the response of the photoelectric device to light of different wavelengths, thereby improving its sensitivity. On the other hand, the wider light absorption range means that more photons are absorbed, leading to increased carrier generation. Meanwhile, the characteristics of the heterojunction structure effectively enhance both carrier separation and transport efficiency. Combined with these factors, the total performance efficiency of optoelectronic devices can be significantly improved. In research on self-powered photodetectors, enhancing the solar energy absorp-

tion of 2D materials represents a central challenge in the field of self-powered photodetection.[43] The optimization of light absorption performance in PtSSe/AlN heterostructures provides stronger support for the development of self-powered photodetectors.

3.3.4. Biaxial strain dependence of the PtSSe/AlN heterostructure band structure

The band gap of a material can be controlled by biaxial strain. For semiconductor materials,[44,45] increasing the band gap can improve the breakdown voltage and thermal stability of devices; decreasing the band gap can enhance the absorption of long-wavelength light, which meets the needs of different optoelectronic devices, such as adjusting the response of solar cells to different spectra.[46] Biaxial strain was applied to the PtSSe/AlN heterostructure along the zigzag and armchair directions, with magnitudes of −8% to 8% biaxial strain applied to the PtSSe/AlN heterojunction, respectively, in equal proportions at 2% intervals. The electronic behavior and band alignment of the PtSSe/AlN heterostructure under biaxial strain are summarized in Fig. 6.

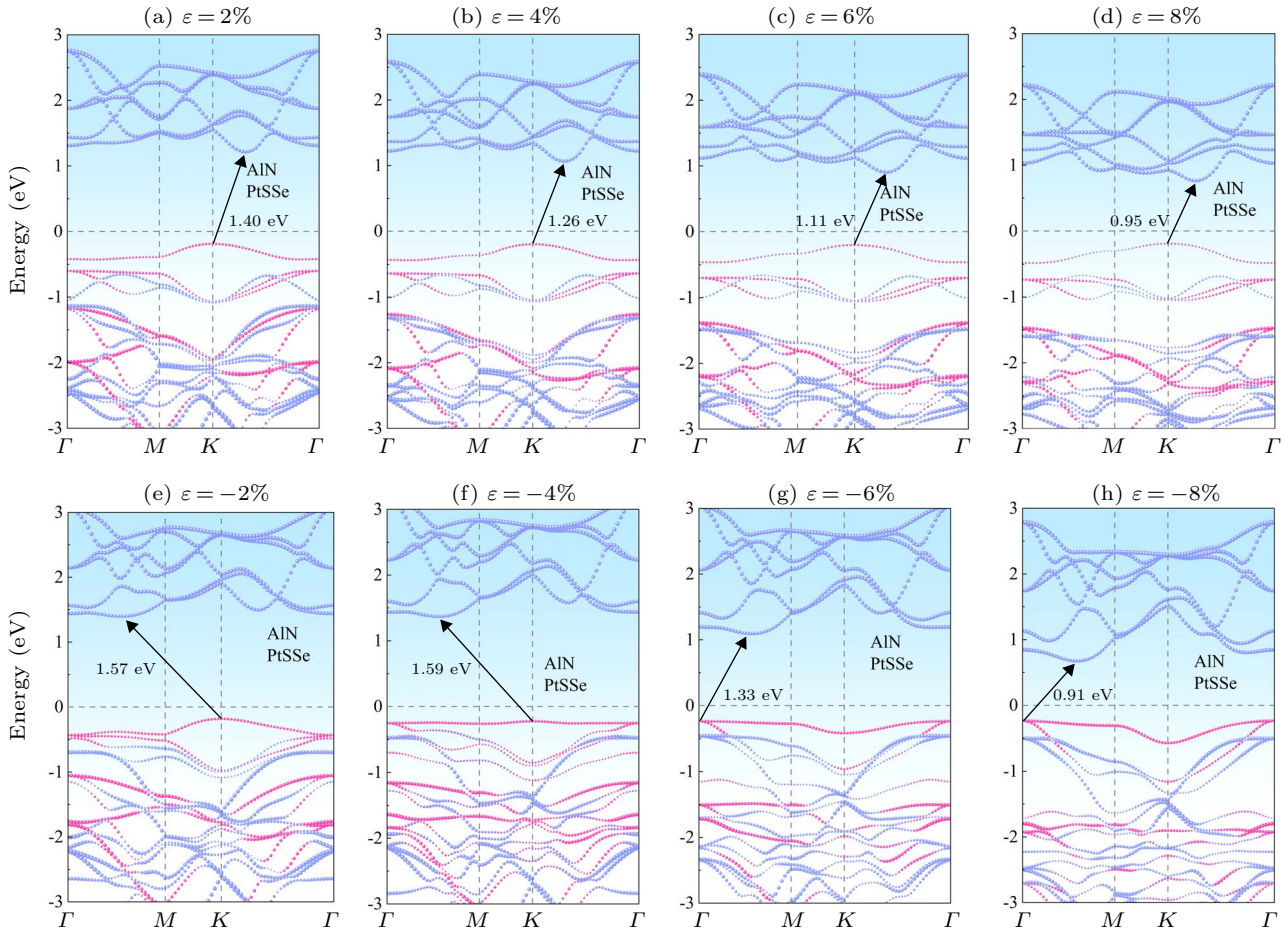


Fig. 6. (a)–(h) How the PtSSe/AlN bands shift under step-by-step biaxial strain. Stretching and compression are used to represent the applied strain.

The calculations reveal that the bandgap of the PtSSe/AlN stack can be anywhere between 0.919 eV and 1.59 eV after applying –8% to 8% biaxial strain to the PtSSe/AlN heterojunction as described. The application of tensile strain induces a variation in the band gap from 0.95 eV to 1.40 eV. The electronic evolution depicted in Figs. 6(a)–6(d) reveals that the CBM moves downward in response to increasing tensile strain whereas the VBM shows minimal shift. Consequently, the band gap narrows. When compressive strain is applied, the band gap of this heterojunction can be modulated from 0.91 eV to 1.59 eV. Figures 6(e)–6(h) show that the conduction band bottom moves to the left and gradually increases with an increase in the compressive strain, while the valence band top remains basically unchanged, resulting in an increase in the band gap. Furthermore, it was observed that the PtSSe/AlN heterostructure maintained its type-II band alignment under the application of biaxial strain, indicating that the heterostructure possesses high stability under biaxial strain conditions. The band structure of type-II semiconductors typically exhibits unique carrier separation characteristics, and strain does not alter its band type. This indicates that the photogenerated carrier separation efficiency in PtSSe/AlN heterojunctions remains largely unaffected, making them suitable for stable use in high-efficiency solar cells and high-performance optoelectronic detectors.

3.4. Self-powered photodetector based on the PtSSe/AlN heterojunction

3.4.1. Model construction of a self-powered photodetector based on the PtSSe/AlN heterostructure

Figure 7 shows a model built from two electrodes sandwiching a 34-atom central scattering zone that is illuminated by both LPL and EPL.

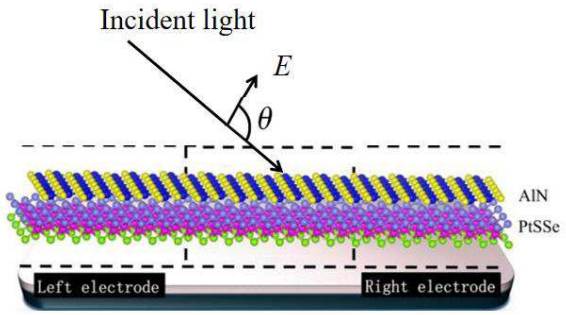


Fig. 7. Schematic of a self-powered photodetector based on a PtSSe/AlN heterojunction.

3.4.2. Photogenerated current density of the self-powered PtSSe/AlN heterostructure photodetector under different polarized lights

Figure 8 shows the photogenerated current density curves of the self-powered PtSSe/AlN photoelectric detector studied and calculated using Nanodcal, where the photon energy range set by the software is 1.2–3.2 eV in 0.2 eV steps, while the polarization angles θ of LPL and EPL are set from 0° to 180° in 15° steps. Figures 8(a) and 8(b) present the photogenerated current density of a self-powered PtSSe/AlN heterojunction photodetector under LPL and EPL irradiation with varying photon energies. Under LPL, the curve peaks at 2.4 eV and the photogenerated current density of the self-powered PtSSe/AlN heterojunction photodetector reaches 0.0609 per photon. Under EPL irradiation, when the photon energy is 2.0 eV the photogenerated current density of the self-powered PtSSe/AlN heterojunction photodetector reaches 0.181 per photon.

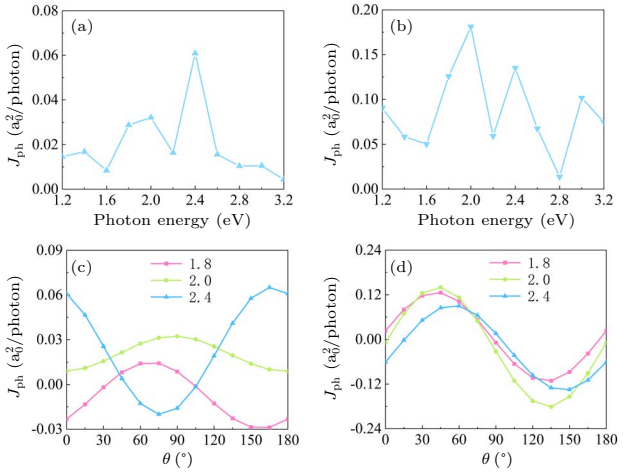


Fig. 8. Photogenerated current density of a self-powered PtSSe/AlN heterojunction photodetector under (a), (c) LPL and (b), (d) EPL.

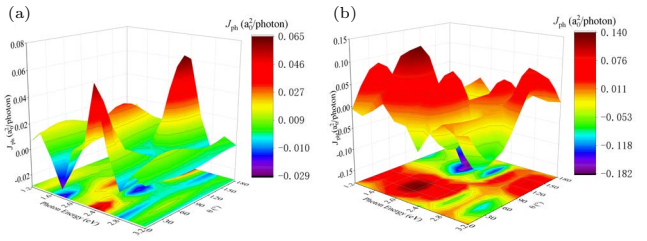


Fig. 9. Power supply of a PtSSe/AlN heterojunction photodetector: (a) photogenerated current density under LPL, (b) photogenerated current density under EPL.

Figures 8(c) and 8(d) show the photogenerated current density curves of self-powered PtSSe/AlN heterojunction photodetectors under LPL and EPL irradiation with varying polarization angles. As can be seen from Fig. 8(c), the photocurrent at 2.0 eV and 2.4 eV follows a clear cosine curve as the polarization angle changes. Specifically, with LPL irradiation, for 2.4 eV photons, the photoelectric current density achieves its maximum at a polarization angle of 165°. This matches Fig. 9(a). Likewise, Fig. 8(d) shows that the photogenerated current density of the heterojunction has a sinusoidal variation trend with change in polarization angle under any photon energy condition. Specifically, under EPL irradiation, at 2.0 eV photon energy the photocurrent peaks at a polarization angle of 135°, as plotted in Fig. 9(b). In short, the PtSSe/AlN heterojunction delivers distinct current levels for each photon energy, and keeping the energy fixed while sweeping θ still alters the photocurrent.

3.4.3. Polarization sensitivity of the self-powered PtSSe/AlN heterostructure photodetector

In order to find out the polarization sensitivity of the self-powered PtSSe/AlN heterojunction photodetector, the extinction ratio of the photodetector was computed and defined as $R_{\parallel}/R_{\perp}$, where $R_{\parallel}$ and $R_{\perp}$ represent the photocurrent density for 0° and 90° polarized light, respectively. Figures 10(a) and 10(b) show the extinction ratio of self-powered PtSSe/AlN heterojunction photodetectors under different polarized light conditions (LPL and EPL). Figures 10(a) and 10(b) show that, under both LPL and EPL, the extinction ratio of the self-powered PtSSe/AlN photodetector peaks at about 14 when the photon energy is 2.6 eV and stays high at 3.2 eV. The comparable on/off current ratios under LPL

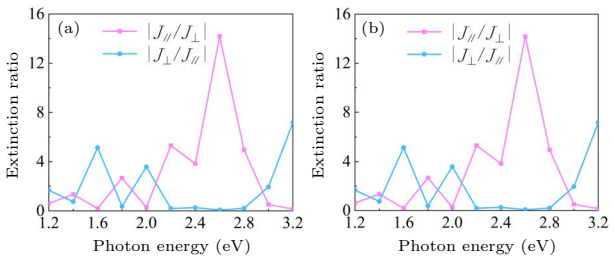


Fig. 10. PtSSe/AlN heterojunction photodetector: (a) absorption ratio under LPL irradiation at different photon energies, (b) absorption ratio under EPL irradiation at different photon energies.

and EPL show that the self-powered PtSSe/AlN photodetector hardly distinguishes polarization. The findings show that the PtSSe/AlN stack works for general photodetectors while its polarization-independent response also suits polarized-light sensors, optical modulators and polarization analyzers.

4. Conclusion

This work focuses on the PtSSe/AlN heterostructure, probing its performance in a self-powered photodetector by examining its electronic, optical, and optoelectronic properties. We used a mix of tools, providing 2D materials with the solid theoretical backup they require for optoelectronics.

(i) The work-function mismatch drives electrons from AlN to PtSSe, creating a built-in field and a sharp interfacial potential step that lowers the injection barrier, speeds carrier diffusion, and boosts the light-to-current conversion efficiency.

(ii) The photoelectric characteristics of self-powered PtSSe/AlN heterojunction photodetectors were studied, and it was found that the heterojunction photodetectors have a large photogenerated current density and a large extinction ratio, achieving a maximum extinction ratio near 14 at 2.6 eV and high contrast at 3.2 eV, irrespective of polarization.

In conclusion, the PtSSe/AlN heterostructure exhibits remarkable stability and efficient charge separation due to its type-II band alignment. It demonstrates enhanced photoelectric conversion through improved light absorption and an internal electric field.

Acknowledgments

Project supported by the National Natural Science Foundation of China Youth Fund (Grant No. 12104362) and the Shaanxi Provincial Innovative Talent Promotion Program — Youth Science and Technology Rising Star Project (Grant No. 2022KJXX-61).

References

[1] Zhao L, Chu X, Cheng J, Wang S, Jin W and Zhang Z 2025 *Front. Phys.* **20** 044301
[2] Olabi A G, Abdelkareem M A, Wilberforce T and Sayed E T 2021 *Renew. Sustain. Energy Rev.* **135** 110026
[3] Li Y Y, Gao B, Han Y, Chen B and Huo J 2021 *Front. Phys.* **16** 43301
[4] Mak K F and Shan J 2016 *Nat. Photonics* **10** 216
[5] Cui Z, Wu H, Bai K, Chen X, Li E, Shen Y and Wang M 2022 *Physica E* **144** 115361
[6] Yang Q, Tan C J, Meng R S, Jiang J K, Liang Q H, Sun X, Yang D G and Chen X P 2016 *IEEE Electron Device Lett.* **38** 145
[7] Hao Y, Wang X and An Y A 2021 *Phys. Scr.* **96** 125835
[8] Liu X, Luo J, Lin Y, Lin Z, Liu X, He J, Yu W, Liu Q, Wei T, Yang J and Zhang W 2021 *ACS Appl. Electron. Mater.* **3** 5415
[9] Xu Z, Zang J, Yang X, Chen Y, Lou Q, Li K, Lin C, Zhang Z and Shan C 2021 *Semicond. Sci. Technol.* **36** 065007
[10] Kumar K, Yadav R, Husale S, Singh P and Kaur D 2022 *Sol. Energy Mater. Sol. Cells* **246** 111942
[11] Ma R, Tan Q, Yang P, Liu Y and Wang Q 2024 *Front. Phys.* **19** 43204
[12] Gao C, Wang Y, Fu S, Song Y, Han Y, Fu R, Wu Z, Cui W, Ma J, Li B and Xu H 2024 *Mater. Today Phys.* **45** 101474
[13] Han Y, Wang Y, Gao C, Fu S, Cui W, Wu Z, Li B, Shen A and Liu Y 2025 *J. Mater. Sci. Technol.* **225** 141
[14] Fan D, Yin M, Wang F, Wang Z, Li H, Hu H, Guo F, Feng Z, Li J, Zhang D and Li Z 2024 *Int. J. Hydrog. Energy* **60** 342
[15] Sattar S and Larsson J A 2020 *ACS Appl. Electron. Mater.* **2** 3585
[16] Zhao X, Niu W, Zhang H, Dai X, Wei S and Yang L 2020 *Appl. Surf. Sci.* **510** 145316
[17] Zhao X, Dang M, Niu W, Zhao Q, Dai X and Wei S 2020 *Physica E* **124** 114254
[18] Jakhar M, Kumar A, Ahluwalia P K, Tankeshwar K and Pandey R 2022 *Materials* **15** 2221
[19] Wang G, Tang W, Xie W, Tang Q, Wang Y, Guo H, Gao P, Dang S and Chang J 2022 *Appl. Surf. Sci.* **589** 152931
[20] Xie L, Wang Z, Zhang Z, Li J, Cheng X, Yuan C and Feng S 2024 *Solid State Commun.* **390** 115621
[21] Pang Q, Qian J J, Tang Y X, Li H, Gao D L, Xie Y and Song Y L 2024 *Mater. Today Commun.* **40** 109685
[22] Wu H, Chen M, Cheng H, Yang T, Zeng M and Yang M 2025 *J. Mater. Inform.* **5** 15
[23] Jamdagni P, Kumar A, Srivastava S, Pandey R and Tankeshwar K 2024 *Int. J. Hydrog. Energy* **66** 268
[24] Sheng Y, Wu Y, Jiang C, Cui X, Mao Y, Ye C and Zhang W 2025 *J. Mater. Inform.* **5** 7
[25] Tu K, Gu J, Lu L, Yuan S, Zhou L and Chen Z 2022 *J. Mater. Inform.* **2** 13
[26] Wang Y, Fu S, Han Y, Gao C, Fu R, Wu Z, Cui W, Li B, Shen A and Liu Y 2025 *Small* **21** 2406989
[27] Han B and Li F 2023 *J. Mater. Inform.* **3** 24
[28] Heyd J, Scuseria G E and Ernzerhof M 2003 *J. Chem. Phys.* **118** 8207
[29] Grimme S, Antony J, Ehrlich S and Krieg H 2010 *J. Chem. Phys.* **132** 154104
[30] Li Y, Kabanova N A, Blatov V A and Wang J 2025 *J. Mater. Inform.* **5** 21
[31] Cui Z, Ren K, Zhao Y, Wang X, Shu H, Yu J, Tang W and Sun M 2019 *Appl. Surf. Sci.* **492** 513
[32] Yin J, Li L, Guo X, Ren J and Lu X 2022 *Chem. Phys.* **563** 111698
[33] Cui Z, Yang K, Ren K, Zhang S and Wang L 2022 *Mater. Sci. Semicond. Process.* **152** 107072
[34] Luo Y, Wang S, Shu H, Chou J P, Ren K, Yu J and Sun M 2020 *Semicond. Sci. Technol.* **35** 125008
[35] Fu Z, Yan P, Li J, He C, Ouyang T, Zhang C, Tang C and Zhong J 2020 *Phys. Status Solidi RRL* **14** 2000395
[36] Nguyen D K, Ponce-Pérez R, Guerrero-Sanchez J and Hoat D M 2024 *RSC Adv.* **14** 19067
[37] Bacaksiz C, Sahin H, Ozaydin H D, Horzum S, Senger R T and Peeters F M 2015 *Phys. Rev. B* **91** 085430
[38] Vo D D, Vu T V, Al-Qaisi S, Tong H D, Le T S, Nguyen C V, Phuc H V, Luong H L, Jappor H R, Obeid M M and Hieu N N 2020 *Superlattices Microstruct.* **147** 106683
[39] Yin G, Lai C K, Chang N, Liang Y, Mao D and Zhou X 2024 *Front. Phys.* **19** 62201
[40] Chen S, Peng Y, Li C and Hou Z 2021 *Int. J. Hydrog. Energy* **46** 32055
[41] Luo S Q, Wang J F, Yang B and Yuan Y B 2019 *Front. Phys.* **14** 53401
[42] Henkelman G, Arnaldsson A and Jónsson H 2006 *Comput. Mater. Sci.* **36** 354
[43] Yang K, Cui Z, Li E, Shen Y, Zhang L, Ma D, Yuan Z, Dong Y and Zhang S 2023 *Chem. Phys.* **571** 111903
[44] Dong H M, Guo S D, Duan Y F, Huang F, Xu W and Zhang J 2018 *Front. Phys.* **13** 137307
[45] Cui Z, Xu H, Wang X, Xia L, Zhang S and Wang L 2026 *Micro Nanostruct.* **212** 208569
[46] Zhou T, Qian G, Huang S, Liang Q, Luo X and Xie Q 2023 *Phys. Lett. A* **480** 128956